Reaction Chemistry & Engineering

Two-Compartment Kinetic Monte Carlo Modelling of Electrochemically Mediated ATRP

Journal:	*Reaction Chemistry & Engineering*
Manuscript ID	RE-ART-08-2018-000156.R1
Article Type:	Paper
Date Submitted by the Author:	30-Aug-2018
Complete List of Authors:	D'hooge, Dagmar; Ghent University, Laboratory for Chemical Technology Fantin, Marco; Carnegie Mellon University, Department of Chemistry Magenau, Andrew; Drexel University Konkolowicz, Dominik; Miami University Matyjaszewski, Krzysztof; Carnegie Mellon University, Department of Chemistry

Two-Compartment Kinetic Monte Carlo Modelling of Electrochemically Mediated ATRP

Dagmar R. D'hooge,[1,2,3*] Marco Fantin,[1] Andrew J. D. Magenau,[1,4] Dominik Konkolewicz,[1,5] Krzysztof Matyjaszewski[1*]

[1]Center for Macromolecular Engineering, Department of Chemistry, Carnegie Mellon University, 4400 Fifth Avenue, Pittsburgh, Pennsylvania 15213, USA

[2]Laboratory for Chemical Technology, Ghent University, Technologiepark 914, Gent, Belgium

[3]Centre for Textiles Science and Engineering, Ghent University, Technologiepark 907, Gent, Belgium

[4]Department of Materials Science and Engineering, Drexel University, Philadelphia, PA 19104, USA

[5]Department of Chemistry and Biochemistry, Miami University, Oxford, Ohio 45056, USA

Corresponding authors:

dagmar.dhooge@ugent.be, km3b@andrew.cmu.edu

Abstract

For electrochemically mediated atom transfer radical polymerization (*e*ATRP), novel mechanistic insights are formulated based on a two-compartment kinetic Monte Carlo model in which catalyst concentration gradients between a large "bulk" compartment away from the electrode and a very small compartment around the electrode are accounted for to reflect the concept of the Nernst diffusion layer. The mass transport of deactivator catalyst to the electrode and its electrochemical reduction at the electrode are treated separately to enable the model to explicitly distinguish between limitations of mass transport and limitations due to intrinsic chemical reactivity. The model is applied to *e*ATRP of methyl acrylate at 298 K with $Cu^{II}Br_2$/Me_6TREN (Me_6TREN: tris((2-dimethylamino)ethyl)amine) and *e*ATRP of *n*-butyl acrylate at 317 K with $Cu^{II}Br_2$/TPMA (TPMA: tris(2-pyridylmethyl)amine). Diffusional limitations on termination need to be accounted for to properly reflect the *e*ATRP kinetics and the microstructural properties of the obtained polymers. In most cases, an *e*ATRP with mixed chemical and mass transport control is obtained.

Keywords: mass transport, controlled radical polymerization, electrochemical reduction, compartment modeling, diffusional limitations

Introduction

Controlled radical polymerization (CRP), also known as reversible deactivation radical polymerization (RDRP), allows for the synthesis of well-defined (co)polymers characterized by a narrow chain length distribution (CLD), a predetermined number average chain length (x_n), and a high degree of livingness.[1-6] The broad utility of CRP has enabled synthetic polymer chemists to create a versatile array of advanced polymeric architectures containing a vast range of polymers with a variety of compositions, functionalities, and topologies.[7-9]

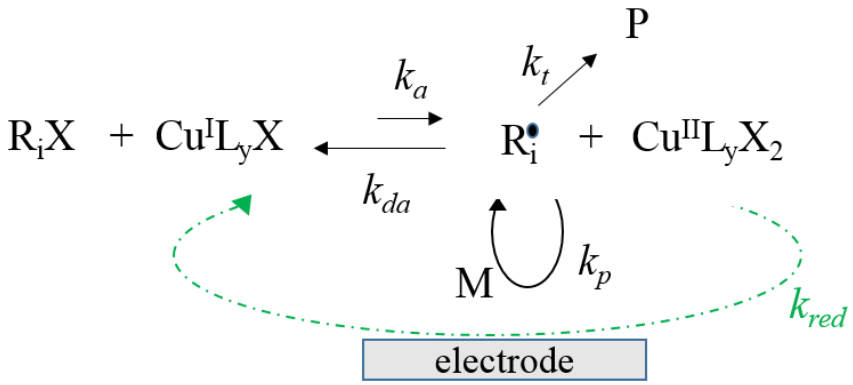

Figure 1: Mechanism of ATRP and *e*ATRP; k_a, k_{da}, k_p, k_{red} (only for *e*ATRP), and k_t represent the rate coefficients of activation, deactivation, propagation, reduction, and termination. R_iX: dormant macromolecules with chain length *i* with special case of *i*=0 referring to the ATRP initiator (then k_{a0} and k_{da0}); R_i: (macro)radical with special case of *i*=0 referring to the ATRP initiator-derived radical; *M*: monomer; *P*: dead polymer molecule; activator (A): Cu^IL_yX; deactivator (DA): $Cu^{II}L_yX_2$; L: ligand; X: halogen.

One of the most versatile CRP techniques is atom transfer radical polymerization (ATRP) which is mediated through a transition metal complex regulating the equilibrium between active macroradicals (R_i; *i*: chain length) and dormant macromolecules (R_iX) *via* a catalytic cycle (Figure 1; without k_{red}). The ATRP equilibrium commonly involves a copper-based low oxidation state catalyst complex/activator (Cu^IL_yX; A) and a higher oxidation state catalyst complex/deactivator ($Cu^{II}L_yX_2$; DA).[2] This equilibrium strongly favors the dormant state, ensuring a concurrent growth of macromolecules, starting from ATRP initiator molecules (R_0X).[10] In a well-controlled ATRP, the radicals will typically add only a few monomer units

before being deactivated again by $Cu^{II}L_yX_2$.[11-13] Concurrently with this activation-growth-deactivation process, however, unavoidable termination reactions[14] occur, resulting in loss of end-group functionality (EGF), accumulation of deactivator, and rate retardation through the well-known persistent radical effect.[15, 16]

Since the discovery of ATRP, significant progress has been made with respect to catalyst design and optimization of reaction conditions. For instance, activators regenerated by electron transfer (ARGET) and initiators for continuous activator regeneration (ICAR) ATRP allowed catalyst concentrations to be minimized to parts-per-million (ppm) levels.[17-19] Diminished catalyst concentrations are feasible due to a continuous (re)generation of the activator from the deactivator by employing chemical reducing agents or conventional radical initiators in ARGET and ICAR ATRP, respectively. The catalyst concentration can be greatly reduced without influencing the polymerization rate provided that an adequate and sufficiently high ratio of $[Cu^{I}L_yX]$ to $[Cu^{II}L_yX_2]$ is maintained.[13, 20, 21] For example, D'hooge *et al.*[22, 23] demonstrated that semi-batch ATRPs involving the joint addition of conventional radical initiator, deactivator and/or monomer allow a full exploitation of ICAR ATRP, for the synthesis of both well-defined homopolymers and gradient copolymers.

The more recent development of electrochemically mediated ATRP (*e*ATRP)[24] further contributed to the expansion of these modified ATRP techniques aiming at low catalyst concentrations. The *e*ATRP mechanism is shown in Figure 1 (now with k_{red}) and starts from a state where exclusively deactivator, alkyl halide, and monomer are present. After imposing a predetermined reducing potential *E*, activator species are generated *in situ* by a one-electron reduction at the working electrode. As in normal or conventional ATRP, the activator molecules can react with alkyl halide ATRP initiator molecules (R_0X), forming ATRP-initiator derived radicals (R_0) through an inner-sphere electron-transfer step. The radicals can subsequently propagate, be deactivated to their dormant alkyl halide form, or terminate with any other radical

species. At the working electrode, activator molecules can thus be continuously (re)generated, similar to ARGET and ICAR ATRP, to compensate for termination reactions. This allows for further activation of dormant species and continued propagation until the desired (average) chain length and conversion is achieved.[25]

In the first pioneering study,[24] $Cu^{II}Br_2$/Me_6TREN (Me_6TREN: tris((2-dimethylamino)ethyl)amine) was electrochemically reduced to $Cu^{I}Br$/Me_6TREN to polymerize methyl acrylate (MA) using acetonitrile (MeCN) as solvent and ethyl 2-bromopropionate (EBP) as ATRP initiator. Under these conditions, a well-controlled polymerization process was observed as evidenced by the linear increase in the number average chain length (x_n) with monomer conversion and low dispersities (< 1.2) at high monomer conversions. Electrochemical reduction of copper complexes by the direct insertion of electrons eliminated the need for exogenous reducing agents, thus limiting contamination during polymerization. Initial reports demonstrated that *e*ATRP of acrylates can be successfully carried out utilizing 50 ppm of copper catalyst while maintaining characteristics of a well-controlled polymerization.[24, 26] Subsequent examples extended the *e*ATRP technique to aqueous and dispersed media[27-30] and to a wider range of monomers[31-33] to make complex polymeric architectures.[34, 35] The *e*ATRP technique provides enhanced levels of polymerization control, whereby the magnitude and modulation of the applied potential allowed precise tuning of the polymerization rate and good temporal control by toggling the polymerization on/off at desired intervals.

The *e*ATRP technique has been greatly simplified by utilizing galvanostatic conditions and sacrificial anodes, which eliminates the need for reference electrodes and two-zone reactors.[36] Moreover, efforts to make *e*ATRP more sustainable and practical have been implemented by employing electrodes constructed from non-precious metals,[37, 38] and by purifying polymerizations through electrochemical stripping of metal contaminates from the crude

reaction mixture.[25, 26] In a similar way, other external stimuli have been successfully applied to control ATRP.[39-44]The possibility to reduce/oxidize the catalyst on demand and with precision has also been considered to pattern surfaces, exploiting the catalyst concentration gradients established in the volume close around the electrode surface.[45]

To fully exploit *e*ATRP, the behavior of mass transport near the electrode surface should be better understood to design more accurate polymerizations and surface processes. Ideally, this implies the explicit consideration of the concentration change of catalyst from the main region of the solution (value C_b) to the surface (value C_s), as depicted by blue line in Figure 2 (left). In the theoretical treatment of electrochemical reactions, this concentration change is approximated by a linear concentration variation in the so-called Nernst diffusion layer (d_N), which is a region near the electrode (dashed black line in Figure 2; left). *e*ATRP is typically carried out under forced convection to minimize d_N and therefore to maximize the concentration gradient between bulk and surface.

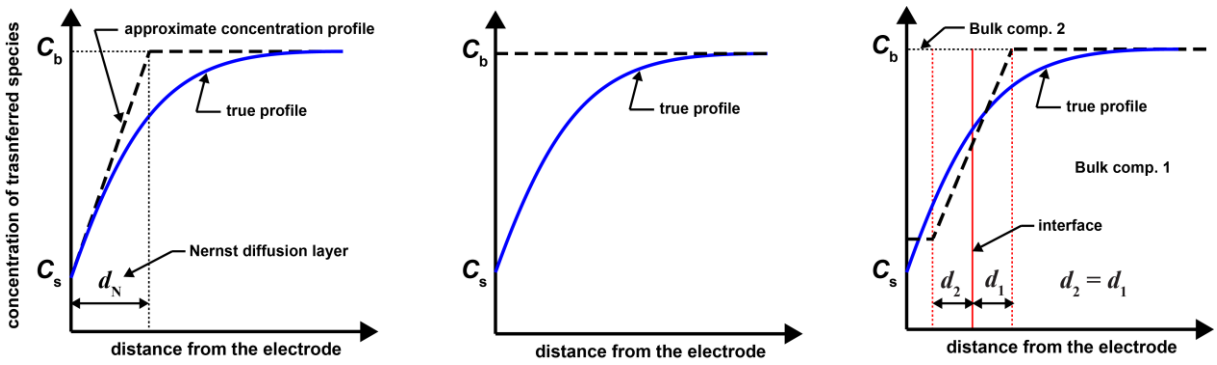

Figure 2: Left: Nernst diffusion layer near an electrode surface with an approximate linear concentration change (dashed black line) with respect to the actual concentration change (blue line) that starts in the bulk (value C_b) and ends at the surface (value C_s); Middle: in a pseudo-homogenous kinetic model, as previously considered,[46] C_b is used at all distances (horizontal dashed black line) and an apparent rate coefficient is needed to describe the electrochemical reduction, *i.e.* a time dependent coefficient is needed to compensate for the deviation from the Nernst diffusion layer concept; Right: transport model in the present work in which two compartments (one away from the electrode (# 1) and one close around the electrode (# 2)) with "bulk" concentrations are separated from each other with two film layers (edges: dashed red lines; (virtual) interface: full red line). Here special case of identical layer thicknesses: $d_1=d_2=d$ and the same equilibrium concentrations at the interface. The volume of the second compartment is very small so this model should be in a close agreement with the Nernst diffusion layer concept.

In original kinetic modeling studies the catalyst concentration gradient in *e*ATRP (*cf.* Figure 2; left) was captured in a formal manner. Guo *et al.*[46] performed the first kinetic modeling study of solution *e*ATRP, selecting *n*-butyl acrylate (*n*BuA) as monomer, tris(2-pyridylmethyl)amine (TPMA) as ligand, ethyl 2-bromoisobutyrate (EBiB) as ATRP initiator, and a polymerization temperature of 317 K. Through a deterministic method of moments, hence based on differential equations, these authors reported a set of rate coefficients allowing the description of average *e*ATRP characteristics. For simplicity, these authors assumed that diffusional limitations on termination can be neglected. Moreover, they used a pseudo-homogeneous model (Figure 2; middle) to describe the electrochemical reduction with all differential equations written for one compartment with a size equal to the total reaction volume *V*. In this model, the bulk catalyst concentration is computed conventionally, but using a correction factor to compensate for the omission of the Nernst diffusion layer concept. The inherent heterogeneous nature of the electrochemical approach is thus implicitly reflected, and the electrochemical reduction reactivity is treated as an apparent one that is rescaled with respect to a maximal reduction coefficient and can be time-dependent. Despite its assumptions, the pseudo-homogeneous model was effectively applied to highlight that the *e*ATRP rate follows a square root dependence on the catalyst loading, and only in limiting cases of very negative applied potential a mass-controlled regime is reached. In a follow-up kinetic modeling study,[31] the same authors applied this deterministic model to describe iron-based *e*ATRP, for which it was shown that slow ATRP initiation can influence the control over the average chain length. Very recently these authors considered theoretical derivations to confirm the strong effect of the electrolyte type on the ATRP equilibrium.[37]

In this work, the kinetics of *e*ATRP are further studied by employing a more detailed two-compartment modeling strategy that more closely resembles the Nernst diffusion layer concept (Figure 2; right). A differentiation is made between (i) (de)activator molecules located in a

compartment away from the electrode, referred to as the "first" compartment, with "bulk" concentrations, and (ii) (de)activator molecules close to the electrode in a small "second" compartment, with "bulk" concentrations similar to the surface concentrations. In that way, the model accounts for differences in catalyst concentrations and for a "resistance" due to mass transport between the two compartments. In the model, the influence of diffusional limitations on termination is also accounted for, so that all possible transport limitations can be evaluated. The kinetic description is performed with a stochastic kinetic Monte Carlo (*k*MC) solver to highlight the capability of this type of solver to cover multi-compartment systems within realistic simulation times scales (second to minute scale) and to extend its RDPR/CRP scope.

The two-compartment *k*MC model is considered to investigate fundamental aspects about the *e*ATRP mechanism, such as whether the process is chemically or mass-transport controlled under typical reaction conditions. The model is compared to experimental data[24, 26] on monomer conversion, x_n, and dispersity for (i) *e*ATRP of MA in MeCN at 298 K with $Cu^{II}Br_2$/Me_6TREN as deactivator and (ii) *e*ATRP of *n*BuA in dimethylformamide (DMF) at 317 K with $Cu^{II}Br_2$/TPMA as deactivator.

Results and discussion

Two-compartment model development

As shown in Figure 3, the reaction mixture (volume *V*) is divided into two compartments, *i.e.* a small volume close to the electrode designated V_2, and a second large volume away from the electrode representing the remaining volume ($V_1 = V\text{-}V_2$). The small compartment can be considered as a very small region directly outside the electrode with a thickness (*d*) similar to that of the Nernst diffusion-layer (d_N) at each side of the electrode surface. It is assumed that d_N remains intact because of the constant stirring applied during *e*ATRP. Hence, based on a typical value for d_N, *i.e.* 5×10^{-6} m,[47] and a typical area for one side of the electrode (*S*), *i.e.* 1.5×10^{-2}

dm^2,[24] V_2 can be assessed as 2×10^{-3} mL. Since for a typical experiment V is *ca.* 20 mL, the volume ratio ($r_V = V_1\ V_2^{-1}$) can be approximated as 10^{-4}.

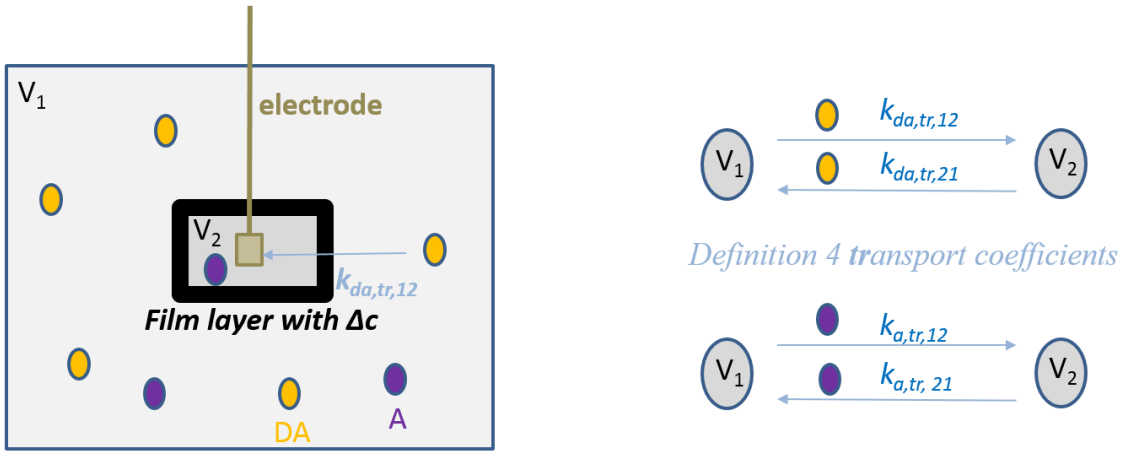

Figure 3: Left: Principle of two-compartment modeling strategy[48] to account for possible mass-transport limitations for the catalyst species (DA: deactivator; A: activator) involved in the electrochemical reduction in *e*ATRP; volume of the reaction mixture *V* is the sum of V_1 and V_2, *i.e.* the volumes of the individual compartments; focus is here restricted to the diffusion of deactivator from V_1 to V_2 (blue arrow), which is characterized by a transport coefficient $k_{da,tr,12}$ (Equation (1)); Right: definition of all 4 transport coefficients (Equation (1)-(2)); each transport coefficient is calculated using the film layer concept as introduced in Figure 1 (right) to reflect the Nernst diffusion layer concept (Figure 1; left); formulas derived in Section S1 of the Supporting Information.

The two compartments in Figure 3 are considered to account for catalyst concentration gradients, which have been reported for heterogeneous catalytic polymerizations and electrochemical systems.[47-50] Since the electrode surface is at a fixed location in the reaction mixture, mass transport can become the limiting factor for the activator (re)generation, justifying the division of the working solution into two compartments. The typical ATRP reactions, *e.g.* (de)activation, propagation, and termination, are assumed to predominantly take place in the first compartment, whereas the electrochemical reduction can only take place if deactivator molecules reach the electrode surface in the second compartment.

This diffusion process, as marked with a blue arrow in Figure 3 (left), is influenced by the diffusivity of the deactivator species and the concentration gradient between the compartments. As introduced in Figure 2 (right), in the present work, a film layer model is employed that

resembles the Nernst layer diffusion concept (Figure 2; left). A deviation is still that an average concentration is modeled in the small compartment (the bulk value for this compartment) so that the surface concentration cannot be exactly extracted but it is close to this average value. According to a film layer description (Figure 2; right), as explained in Section S1 of the Supporting Information, the transport rate coefficients (units: L mol^{-1} s^{-1}) to describe the exchange of a molecule *N* (in this context activator (A) or deactivator (DA)) can be calculated from:[51, 52]

$$k_{N,tr,12} = 2SN_AK_N \quad (1)$$

$$k_{N,tr,21} = \Gamma_N k_{N,12} \quad (2)$$

in which the subscripts "12" and "21" reflect the movement from compartment 1 to 2 and *vice versa*, N_A is the Avogadro constant, Γ_N is the partition coefficient between the large and small compartment (ratio of equilibrium concentrations; here value of 1), and K_N is the overall mass transport coefficient depending on the diffusion coefficients (units: dm s^{-1}; definition Equation (S3) in the Supporting Information). Taking into account the nature of the work, K_N is assumed constant and equal for the activator and deactivator, which have comparable diffusivities under typical ATRP conditions.[53, 54] Hence, out of the four transport coefficients, *i.e.* $k_{a,tr,12}$, $k_{a,tr21}$, $k_{da,tr,12}$, and $k_{da,tr,21}$ (Equation (1)-(2)), only one needs to be determined.

In the present work, $k_{da,tr,12}$ is taken as the reference transport rate coefficient due to its direct link with the subsequent reduction step. This coefficient can be measured under conditions in which a mass-controlled regime is experimentally established. This regime results for the *e*ATRPs carried out at the more negative potentials for the *n*BuA/Cu^{I}TPMA^{+} case, where identical polymerization kinetics was obtained upon a further shift of the potential to more negative values. Under such conditions, an average value of 10^4 L mol^{-1} s^{-1} is obtained for

$k_{da,tr,12}$. This value reflects the typical transport characteristics of a batch mL scale reaction mixture, with an expected accuracy within one order of magnitude.

Table 1: Overview of reactions for the *e*ATRP kinetic model and the corresponding rate coefficients at 298 K (methyl acrylate (MA)/Me$_6$TREN case; EBP; MeCN) and 317 K (*n*-butyl acrylate (*n*BuA)/TPMA case; EBiB; DMF); all reactions except the electrochemical reduction are assumed to take place in the large compartment (Figure 2); *t*: tertiary species (otherwise: secondary); *A*: activator; *DA*: deactivator.

Reaction		***k* at 298 K ((L mol^{-1}) s^{-1}) MA/Me$_6$TREN**	***k* at 317 K ((L mol^{-1}) s^{-1}) *n*BuA/TPMA**	**Ref.**
ATRP	$R_0X + A \xrightarrow{k_{a0}} R_0 + DA$	4.0×10^3	8.0×10^2	55-57a
(de)activation	$R_0 + DA \xrightarrow{k_{da0}} R_0X + A$	5.0×10^7	6.0×10^7	55a
	$R_iX + A \xrightarrow{k_a} R_i + DA$	4.0×10^3	4.0×10^2	55-57a
	$R_i + DA \xrightarrow{k_{da}} R_iX + A$	5.0×10^7	6.0×10^7	55a
	$R_{i,t}X + A \xrightarrow{k_{a,t}} R_{i,t} + DA$	2.0 k_a	2.0 k_a	58b
	$R_{i,t} + DA \xrightarrow{k_{da,t}} R_{i,t}X + A$	0.5 k_{da}	0.5 k_{da}	58b
Electrochemical reduction[d]	$DA \xrightarrow{k_{red}} A$	Equation (3)	Equation (4)	
Chain initiation	$R_0 + M \xrightarrow{k_{p0}} R_1$	10 k_p	k_p[e]	59
Propagation	$R_i + M \xrightarrow{k_p} R_{i+1}$	1.3×10^4	2.7×10^4	59, 60
	$R_{i,t} + M \xrightarrow{k_{p,t}} R_{i+1}$	10^{-3} k_p	10^{-3} k_p	59b
Backbiting	$R_i \xrightarrow{k_{bb}} R_{i,t}$	1.0×10^2	1.0×10^2	61c
Termination by combination[f]	$R_0 + R_0 \xrightarrow{k_{tc,app,00}} P_0$	1.0×10^9	1.0×10^9	62
	$R_0 + R_i \xrightarrow{k_{tc,app,0i}} P_i$	1.0×10^9	1.0×10^9	62
	$R_i + R_j \xrightarrow{k_{tc,app,ij}} P_{i+j}$	1.0×10^9	1.0×10^9	62

[a]within literature range, with more active system for Me$_6$TREN; [b]correction factor in agreement with literature; [c]typical order of magnitude; [d] the related transport coefficient for deactivator ($k_{da,tr,12}$) is has an average value of 10^4 L mol^{-1} s^{-1}; same values for other transport coefficients (Figure 3; right) as partition coefficient of 1 and similar diffusivities for activator and deactivator to a first approximation [e] for simplicity equal, although even a lower value is expected as a tertiary ATRP initiator is employed; [f]apparent rate coefficients to account for diffusional limitations: parameters based on RAFT-CLD-T technique[62] (Supporting Information) with in table value for termination between unimer radicals; terminations with tertiary species are not shown for simplicity but accounted for with literature[63] correction factors of 10 (end/mid) and 100 (mid/mid);

Table 1 gives an overview of the reactions in the *k*MC model, consistent with the reaction scheme applied by Guo *et al.*[46] in their deterministic modeling study of solution *e*ATRP of *n*BuA. A distinction can be made between those reactions specific to ATRP and electrochemistry, leading to a first group of reactions, and those specific to free radical polymerization (FRP), leading to a second group of reactions. In the former group, traditional activation/deactivation reactions and electrochemical reduction are considered, whereas propagation, backbiting, and termination by combination are included in the latter group. Since backbiting is included, secondary and tertiary species are differentiated. Termination by disproportionation, chain transfer to monomer and to polymer, and βC-scission reactions are neglected based on previous literature reports.[64, 65]

The rate coefficients at 298 K (MA/Me_6TREN case) and at 317 K (*n*BuA/TPMA case) are also specified in Table 1 and are in agreement with literature data.[55, 56 58, 61-63, 66] In particular, the ATRP initiator activation rate coefficient (MA/Me_6TREN case) is within the literature range of 2.8 x 10^1 to 3.7 x 10^4 L mol^{-1} s^{-1} (solvent: MeCN)[55-57] and close to value reported by Fantin *et al.*[57] (2.1 x 10^3 L mol^{-1} s^{-1}). The ATRP deactivation rate coefficients are in a similar order of magnitude to the work of Tang *et al.*[55] The activation/deactivation coefficients of TPMA are lower than those with Me_6TREN, consistent with literature data.[67] The ATRP activation and deactivation reactivity of those groups are considered respectively two times higher and lower than the secondary ones, which is in agreement with correction factors up to 10 reported in literature.[58, 63]

For termination, apparent rate coefficients are used with the value for secondary radicals (chain length 1) given in Table 1, neglecting for simplicity the possible impact of catalytic radical termination (CRT),[68] and taking into account that the dominant mode of termination is combination.[68] Several kinetic modeling studies on normal, ARGET and ICAR ATRP have showed that the observed (average) termination reactivity drops significantly with increasing

chain length and viscosity of the reaction mixture upon polymer formation.[69-72] Hence, chain length and conversion dependent apparent termination rate coefficients need to be ideally considered in ATRP kinetic modeling studies to allow for an accurate simulation of the monomer conversion profile and polymer characteristics.[53, 73] Such detailed description is often overlooked, leading to a biased interpretation of CRP mediating agents. In this work, apparent termination rate coefficients based on the so-called reversible addition fragmentation chain transfer-chain length dependent-termination (RAFT-CLD-T) method[62, 66] are used, while correcting for the presence of solvent. These coefficients have been determined at 323 K and for poly(*n*BuA) radicals but it can be expected that they are also representative for poly(MA) radicals at the studied polymerization temperature of 298 K. For the other reaction steps, at least to a first approximation, diffusional limitations can be neglected based on literature data, taking into account that the maximum simulated conversion is limited to 0.80.[53] As a result of the parameters available in the literature or judiciously approximated, only the value of k_{red} is thus refined in the *k*MC model at different potentials.

Contribution of chemical reduction at the electrode

Figure 4(a)-(c) show the comparison between simulated and experimental results for the *e*ATRP of the MA/Me_6TREN case ($[M]_0$:$[R_0X]_0$:$[Deact]_0$ = 500:1:0.025; 50% MeCN; T= 298 K[24]). To be consistent with more recent *e*ATRP conventions, all values of applied potential are reported as overpotential (ΔE) values. These are defined as the difference between the applied potential, E_{app}, and the halfwave potential of the copper complex, $E_{1/2}$, hence, $\Delta E = E_{app} - E_{1/2}$. Therefore, the three analyzed cases for Me_6TREN are ΔE = -0.03 V (red dotted lines), 0 V (green dashed lines), and 0.03 V (full blue lines). Analogous results for the *n*BuA/TPMA case ($[M]_0$:$[R_0X]_0$:$[Deact]_0$ = 300:1:0.09; 317 K) are provided in Figure 5(a)-(b). More negative, hence, more reducing potentials result in higher polymerization rates (Figure 4(a) and Figure 5(a)) but lead to nearly identical control over chain length as illustrated by their similar x_n and

dispersity values in Figure 4(b)-(c) and Figure 5(b)-(c). For all potentials, the "livingness" (preservation of chain ends) remains very high, with values above 99% (Figure 4(d) and Figure 5(h)).

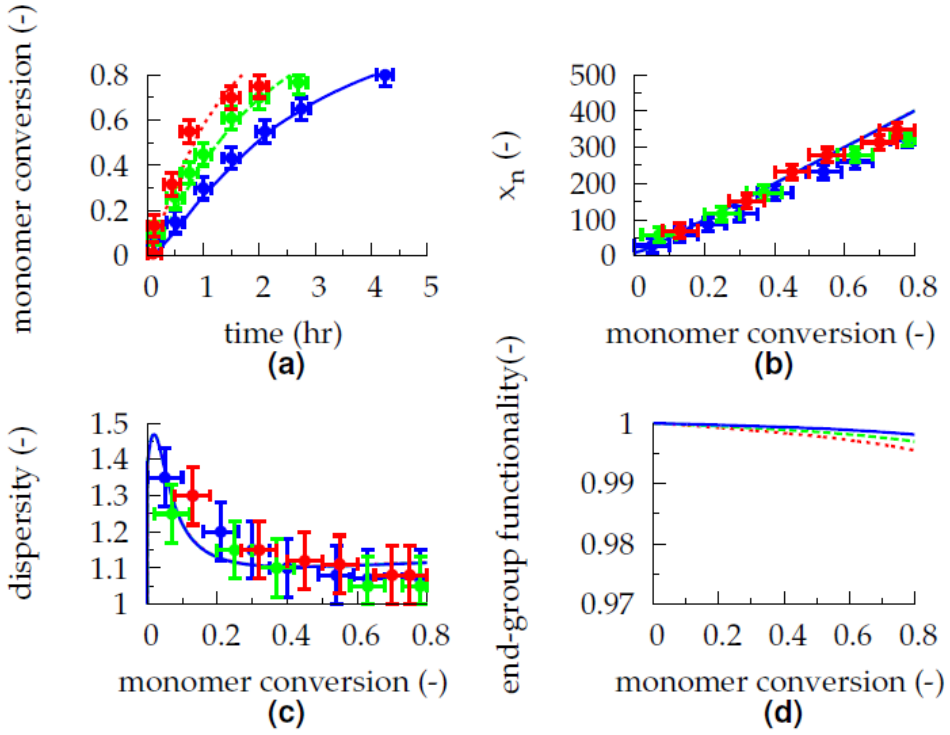

Figure 4: Methyl acrylate/Me$_6$TREN case: (a) Monomer conversion as a function of time; (b) number average chain length (x_n); (c) dispersity; (d) end-group functionality (EGF); reaction conditions: [M]$_0$:[R$_0$X]$_0$:[Deact]$_0$ = 500:1:0.025; 50% solvent (vol); T = 298 K; red dotted/green dashed/blue full lines: ΔE = -0.03/0/0.03 V; experimental data for (a)-(c): Magenau e*t al.*[24] with typical average error bars.

The most sensitive response for the tuning of k_{red} are therefore the monomer consumption data (Figure 4(a) and Figure 5(a)) as the strongest deviations are there recorded both experimentally and theoretically. For the MA/Me$_6$TREN case, regression analysis of the tuned k_{red} values reveals an exponential dependency with a value of 0.1 s^{-1} at ΔE = 0.03 V and a value of 6.6 s^{-1} at ΔE = -0.03 V:

$$k_{red} = 8.5\ 10^{-1}(s^{-1})\ \exp(-64.2\ \Delta E) \quad (3)$$

Similarly, for the *n*BuA/TPMA$^+$ case the following equation is obtained:

$$k_{red} = 7.0\ 10^{-2}(s^{-1})\ \exp(-23.3\ \Delta E) \quad (4)$$

Such exponential dependencies for k_{red} indicate that indeed a chemical/intrinsic reactivity is determined in the small second compartment, as this dependence agrees with the Nernst law, which predicts an exponential relation between the applied potential and the ratio of Cu^{I} and Cu^{II} at the electrode surface.[74]

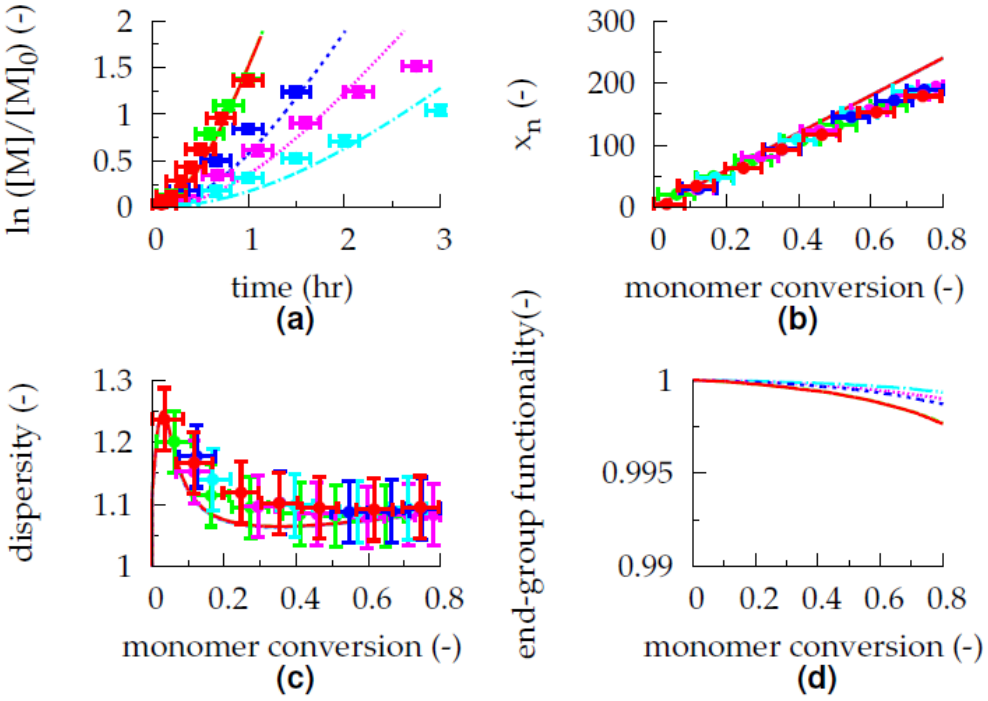

Figure 5: Similar figure as Figure 4 for *n*-butyl acrylate/$TPMA^{+}$ case; reaction conditions: $[M]_0:[R_0X]_0:[Deact]_0$ = 300:1:0.09; 317 K; $[M]_0$=3.9 mol L^{-1}; light blue dashed dotted/ purple dotted/ dark blue dashed/ green full/red full: ΔE = 0/-0.045/-0.085/-0.125/-0.165/-0.180 V; experimental data from Magenau *et al.*[26]

The *k*MC model also gives access to the bulk concentrations in both compartments that are connected which each other through a linear concentration gradient (*cf.* Figure 2; right). The fractions of catalyst in the deactivated state in the large and small compartment are provided in in the Supporting Information. Overall the electrochemical conversion is limited because of the low activator concentration in the bulk of the solution. Furthermore, the high fractions of deactivator in the large compartment in Figure S1 of the Supporting Information suggest that mass transport to/from the bulk of the solution and therefore diffusional limitations plays a role for all the applied potentials.

Contribution of diffusional limitations

For the *n*BuA/TPMA$^+$ case both experiment and theory (Figure 5(a)-(d); coinciding green and red full lines) confirm that too negative potentials lead to identical polymerization results. Hence, a strictly mass-controlled regime is established with diffusion of deactivator to the electrode being the rate determining step. Hence, the question arises at which potential such regime is commenced and in a broader sense in which range of potentials diffusional limitations, hence, transport phenomena, influence the *e*ATRP process.

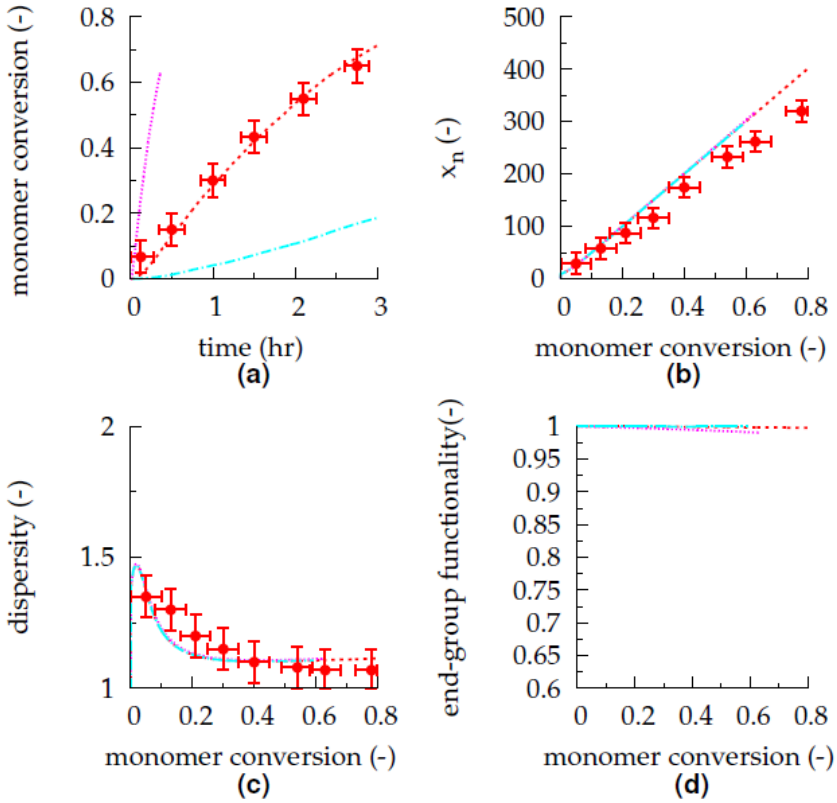

Figure 6: Results for Δ*E* = -0.03 V in Figure 4 (MA/Me$_6$TREN case) with additionally simulation results for a 100 times faster (purple dotted line) or slower (blue dashed line) deactivator transport; in this sensitivity analysis differentiations are recorded with respect to the red line, implying that diffusional limitations and chemistry matter for the reduction.

To address these questions the developed kinetic modeling platform was applied. For example, Figure 6 (MA/ME$_6$TREN case) represents the simulation outcome for a Δ*E* = -0.03 V (red line taken from Figure 4(a)-(d)) if formally so for sensitivity purposes the supply of deactivator

molecules to the electrode surface is enhanced and reduced by respectively increasing (purple dotted line) and lowering (blue dashed dotted line) the transport coefficient $k_{Deact,12}$ (Equation (1)) by a factor 100. Since the purple line is well-above the red line in Figure 6(a), the actual reduction rate for the MA/ME_6TREN case is determined by both diffusion/transport and chemical reactivity. For the theoretical case of a much slower deactivator transport, the polymerization rate is consistently reduced (blue *vs.* red line in Figure 4(a)) and diffusion/transport becomes more dominant.

It therefore follows that the compartment modeling strategy – in combination with the film layer model - allows to generally map whether the reduction rate is in the chemically controlled regime, the mass-controlled regime, or in the transition from one regime to the other, the latter being the case for the MA/Me_6TREN case in the considered ΔE range. The *n*BuA/TPMA case, instead, showed a transition between the mixed and the mass-controlled regime. Note that a one-compartment model is in this context not recommended as at most it can only formally capture these trends through a pure fitting, without explicitly separating transport from chemistry effects.

It should however be stressed that in any case the role of diffusional limitations on the observed termination rate cannot be ruled out. As shown in Figure S3 in the Supporting Information, diffusional limitations on termination have a strong impact on the monomer conversion profile, dispersity variation, and livingness. As the apparent termination reactivity drops with increasing monomer conversion, the polymerization rate increases and the loss of EGF is minimized. Hence, a proper tuning of k_{red} and a design of the *e*ATRP process is only possible if diffusional limitations on termination are properly accounted for, as performed in the present work.

Conclusions

The developed two-compartment kinetic Monte Carlo model in combination with a film layer description can be used to model the *e*ATRP kinetics and control over polymer properties, while acknowledging the heterogeneous nature of the chemical process. No time-dependent apparent reduction parameters are required as the Nernst diffusion layer concept can be incorporated. For too slow transport of deactivator to the electrode, the reduction of the deactivator becomes mass-controlled, whereas in other cases a reaction with mixed chemical-mass transport control is obtained.

Acknowledgments

D.R.D acknowledges the Fund for Scientific Research Flanders (FWO) through a postdoctoral fellowship. This work is also supported by the NSF (CHE 170749).

References

1. J. Nicolas, Y. Guillaneuf, C. Lefay, D. Bertin, D. Gigmes and B. Charleux, *Prog. Polym. Sci.*, 2013, **38**, 63-235.
2. K. Matyjaszewski and J. H. Xia, *Chem. Rev.*, 2001, **101**, 2921-2990.
3. W. A. Braunecker and K. Matyjaszewski, *Prog. Polym. Sci.*, 2007, **32**, 93-146.
4. A. D. Jenkins, R. G. Jones and G. Moad, *Pure Appl. Chem.*, 2010, **82**, 483-491.
5. J. Chiefari, Y. K. Chong, F. Ercole, J. Krstina, J. Jeffery, T. P. T. Le, R. T. A. Mayadunne, G. F. Meijs, C. L. Moad, G. Moad, E. Rizzardo and S. H. Thang, *Macromolecules*, 1998, **31**, 5559-5562.
6. J. S. Wang and K. Matyjaszewski, *J. Am. Chem. Soc.*, 1995, **117**, 5614-5615.
7. K. Matyjaszewski and N. V. Tsarevsky, *Nature Chemistry*, 2009, **1**, 276-288.
8. K. Matyjaszewski, *Adv. Mater.*, 2018, **30**, 22.
9. K. Matyjaszewski and N. V. Tsarevsky, *J. Am. Chem. Soc.*, 2014, **136**, 6513-6533.
10. K. Matyjaszewski, *Macromolecules*, 2012, **45**, 4015-4039.
11. S. K. Fierens, P. H. M. Van Steenberge, M. F. Reyniers, G. B. Marin and D. R. D'Hooge, *Aiche Journal*, 2017, **63**, 4971-4986.
12. S. K. Fierens, S. Telitel, P. H. M. Van Steenberge, M. F. Reyniers, G. B. Marin, J. F. Lutz and D. R. D'Hooge, *Macromolecules*, 2016, **49**, 9336-9344.
13. P. Krys and K. Matyjaszewski, *European Polymer Journal*, 2017, **89**, 482-523.
14. M. J. Zhong and K. Matyjaszewski, *Macromolecules*, 2011, **44**, 2668-2677.
15. H. Fischer, *Chem. Rev.*, 2001, **101**, 3581-3610.
16. M. Souaille and H. Fischer, *Macromolecules*, 2002, **35**, 248-261.
17. K. Matyjaszewski, W. Jakubowski, K. Min, W. Tang, J. Y. Huang, W. A. Braunecker and N. V. Tsarevsky, *Proc. Natl. Acad. Sci. U. S. A.*, 2006, **103**, 15309-15314.
18. N. V. Tsarevsky and K. Matyjaszewski, *Chem. Rev.*, 2007, **107**, 2270-2299.

19. D. Konkolewicz, A. J. D. Magenau, S. E. Averick, A. Simakova, H. K. He and K. Matyjaszewski, *Macromolecules*, 2012, **45**, 4461-4468.
20. D. R. D'hooge, P. H. M. Van Steenberge, P. Derboven, M.-F. Reyniers and G. B. Marin, *Polym. Chem.*, 2015, **6**, 7081-7096.
21. E. Mastan, X. Li and S. Zhu, *Prog. Polym. Sci.*, 2015, **45**, 71-101.
22. D. R. D'hooge, P. H. M. Van Steenberge, M. F. Reyniers and G. B. Marin, *Polymers*, 2014, **6**, 1074-1095.
23. D. R. D'hooge, D. Konkolewicz, M. F. Reyniers, G. B. Marin and K. Matyjaszewski, *Macromol. Theory Simul.*, 2012, **21**, 52-69.
24. A. J. D. Magenau, N. C. Strandwitz, A. Gennaro and K. Matyjaszewski, *Science*, 2011, **332**, 81-84.
25. P. Chmielarz, M. Fantin, S. Park, A. A. Isse, A. Gennaro, A. J. D. Magenau, A. Sobkowiak and K. Matyjaszewski, *Prog. Polym. Sci.*, 2017, **69**, 47-78.
26. A. J. D. Magenau, N. Bortolamei, E. Frick, S. Park, A. Gennaro and K. Matyjaszewski, *Macromolecules*, 2013, **46**, 4346-4353.
27. N. Bortolamei, A. A. Isse, A. J. D. Magenau, A. Gennaro and K. Matyjaszewski, *Angew. Chem.-Int. Edit.*, 2011, **50**, 11391-11394.
28. M. Fantin, A. A. Isse, A. Gennaro and K. Matyjaszewski, *Macromolecules*, 2015, **48**, 6862-6875.
29. Y. Wang, F. Lorandi, M. Fantin, P. Chmielarz, A. A. Isse, A. Gennaro and K. Matyjaszewski, *Macromolecules*, 2017, **50**, 8417-8425.
30. M. Fantin, P. Chmielarz, Y. Wang, F. Lorandi, A. A. Isse, A. Gennaro and K. Matyjaszewski, *Macromolecules*, 2017, **50**, 3726-3732.
31. J. K. Guo, Y. N. Zhou and Z. H. Luo, *Macromolecules*, 2016, **49**, 4038-4046.
32. M. Fantin, A. A. Isse, A. Venzo, A. Gennaro and K. Matyjaszewski, *J. Am. Chem. Soc.*, 2016, **138**, 7216-7219.
33. P. Chmielarz, S. Park, A. Simakova and K. Matyjaszewski, *Polymer*, 2015, **60**, 302-307.
34. S. Park, H. Y. Cho, K. B. Wegner, J. Burdynska, A. J. D. Magenau, H. J. Paik, S. Jurga and K. Matyjaszewski, *Macromolecules*, 2013, **46**, 5856-5860.
35. P. Chmielarz, *Chem. Pap.*, 2017, **71**, 161-170.
36. S. Park, P. Chmielarz, A. Gennaro and K. Matyjaszewski, *Angew. Chem.-Int. Edit.*, 2015, **54**, 2388-2392.
37. J. K. Guo, Y. N. Zhou and Z. H. Luo, *Aiche Journal*, 2018, **64**, 961-969.
38. M. Fantin, F. Lorandi, A. A. Isse and A. Gennaro, *Macromol. Rapid Commun.*, 2016, **37**, 1318-1322.
39. X. Pan, M. Fantin, F. Yuan and K. Matyjaszewski, *Chem. Soc. Rev.*, 2018, **47**, 5457-5490.
40. S. Dadashi-Sila and K. Matyjaszewski, *Macromolecules*, 2018, **51**, 4250-4258.
41. Z. H. Wang, Z. H. Wang, X. C. Pan, L. Y. Fu, S. Lathwal, M. Olszewski, J. J. Yan, A. E. Enciso, Z. Y. Wang, H. S. Xia and K. Matyjaszewski, *Acs Macro Letters*, 2018, **7**, 275-280.
42. Z. H. Wang, X. C. Pan, L. C. Li, M. Fantin, J. J. Yan, Z. Y. Wang, Z. H. Wang, H. S. Xia and K. Matyjaszewski, *Macromolecules*, 2017, **50**, 7940-7948.
43. X. C. Pan, M. A. Tasdelen, J. Laun, T. Junkers, Y. Yagci and K. Matyjaszewski, *Prog. Polym. Sci.*, 2016, **62**, 73-125.
44. X. C. Pan, C. Fang, M. Fantin, N. Malhotra, W. Y. So, L. A. Peteanu, A. A. Isse, A. Gennaro, P. Liu and K. Matyjaszewskit, *J. Am. Chem. Soc.*, 2016, **138**, 2411-2425.
45. B. Li, B. Yu, W. T. S. Huck, W. Liu and F. Zhou, *J. Am. Chem. Soc.*, 2013, **135**, 1708-1710.
46. J. K. Guo, Y. N. Zhou and Z. H. Luo, *Aiche Journal*, 2015, **61**, 4347-4357.
47. A. Bard and L. Faulkner, *Electrochemical Methods: Fundamentals and Applications, 2nd Edition*, **2000**.
48. D. Constales, G. Yablonksi, D. R. D'hooge, J. W. Thybaut and G. B. Marin, *Advanced data analysis and modelling in chemical engineering*, 2016, **Elsevier**.

49. D. Maggioris, A. Goulas, A. H. Alexopoulos, E. G. Chatzi and C. Kiparissides, *Comput. Chem. Eng.*, 1998, **22**, S315-S322.
50. J. Pohn, M. Cunningham and T. F. L. McKenna, *Macromol. React. Eng.*, 2013, **7**, 393-408.
51. J. Wieme, D. R. D'hooge, M. F. Reyniers and G. B. Marin, *Macromol. React. Eng.*, 2009, **3**, 16-35.
52. P. A. Mueller, G. Storti and M. Morbidelli, *Chemical Engineering Science*, 2005, **60**, 377-397.
53. D. R. D'hooge, M. F. Reyniers and G. B. Marin, *Macromol. React. Eng.*, 2013, **7**, 362-379.
54. P. B. Zetterlund, *Macromolecules*, 2010, **43**, 1387-1395.
55. W. Tang, Y. Kwak, W. Braunecker, N. V. Tsarevsky, M. L. Coote and K. Matyjaszewski, *J. Am. Chem. Soc.*, 2008, **130**, 10702-10713.
56. C. A. Bell, P. V. Bernhardt and M. J. Monteiro, *J. Am. Chem. Soc.*, 2011, **133**, 11944-11947.
57. M. Fantin, A. A. Isse, N. Bortolamei, K. Matyjaszewski and A. Gennaro, *Electrochim. Acta*, 2016, **222**, 393-401.
58. P. H. M. Van Steenberge, J. Vandenbergh, M. F. Reyniers, T. Junkers, D. R. D'Hooge and G. B. Marin, *Macromolecules*, 2017, **50**, 2625-2636.
59. Y. W. Marien, P. H. M. Van Steenberge, C. Barner-Kowollik, M. F. Reyniers, G. B. Marin and D. R. D'Hooge, *Macromolecules*, 2017, **50**, 1371-1385.
60. C. Barner-Kowollik, S. Beuermann, M. Buback, P. Castignolles, B. Charleux, M. L. Coote, R. A. Hutchinson, T. Junkers, I. Lacik, G. T. Russell, M. Stach and A. M. van Herk, *Polym. Chem.*, 2014, **5**, 204-212.
61. J. Barth, M. Buback, P. Hesse and T. Sergeeva, *Macromolecules*, 2010, **43**, 4023-4031.
62. G. Johnston-Hall and M. J. Monteiro, *J Polym Sci Part A Polym Chem.* , 2008, **46**, 3155-3173.
63. A. N. Nikitin, R. A. Hutchinson, M. Buback and P. Hesse, *Macromolecules*, 2007, **40**, 8631-8641.
64. D. Konkolewicz, S. Sosnowski, D. R. D'hooge, R. Szymanski, M. F. Reyniers, G. B. Marin and K. Matyjaszewski, *Macromolecules*, 2011, **44**, 8361-8373.
65. T. Junkers and C. Barner-Kowollik, *J Polym Sci Part A Polym Chem.*, 2008, **46**, 7585-7605.
66. C. Barner-Kowollik and G. T. Russell, *Prog. Polym. Sci.*, 2009, **34**, 1211-1259.
67. W. Tang and K. Matyjaszewski, *Macromolecules*, 2006, **39**, 4953-4959.
68. T. G. Ribelli, K. F. Augustine, M. Fantin, P. Krys, R. Poli and K. Matyjaszewski, *Macromolecules*, 2017, **50**, 7920-7929.
69. D. R. D'Hooge, P. H. M. Van Steenberge, M. F. Reyniers and G. B. Marin, *Prog. Polym. Sci.*, 2016, **58**, 59-89.
70. A. M. Rabea and S. P. Zhu, *Polymers*, 2015, **7**, 819-835.
71. P. Krys, H. Schroeder, J. Buback, M. Buback and K. Matyjaszewski, *Macromolecules*, 2016, **49**, 7793-7803.
72. O. Delgadillo-Velazquez, E. Vivaldo-Lima, I. A. Quintero-Ortega and S. P. Zhu, *Aiche Journal*, 2002, **48**, 2597-2608.
73. G. Johnston-Hall and M. J. Monteiro, *Macromol. Theory Simul.*, 2010, **19**, 387-393.
74. M. Fantin, F. Lorandi, A. Gennaro, A. A. Isse and K. Matyjaszewski, *Synthesis*, 2017, **49**, 3311-3322.

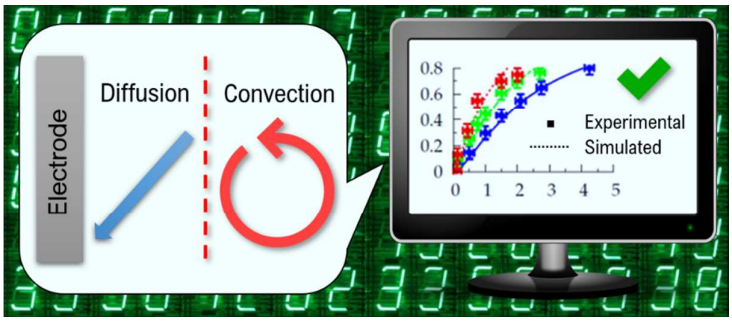

Novel *e*ATRP mechanistic insights are formulated, considering a two-compartment kinetic Monte Carlo model with catalyst concentration gradients accounted for.